All Optic-Fiber Waveguide-Coupled SPR Sensor for CRP Sensing Based on Dielectric Layer and Poly-Dopamine

Jinying MA[1,2,3*], Shixin LI[1], Xiangdong HUANG[2], Junfeng JIANG[3,4], Tianhua XU[3,4,5], and Tiegen LIU[3,4]

[1]*School of Electronic Engineering, Tianjin University of Technology and Education, Tianjin 300222, China*

[2]*School of Electrical and Information Engineering, Tianjin University, Tianjin 300072, China*

[3]*Institute of Optical Fiber Sensing, Tianjin University, Tianjin 300072, China*

[4]*Key Laboratory of Opto-Electronics Information Technology, Ministry of Education, Tianjin 300072, China*

[5]*School of Engineering, University of Warwick, Coventry CV4 7AL, UK*

[*]Corresponding author: Jinying MA E-mail: majinying@tute.edu.cn

Abstract: We developed an all optic-fiber waveguide-coupled surface plasmon resonance (SPR) sensor using zirconium disulfide (ZrS_2) and poly-dopamine (PDA) as the dielectric layer and biological cross-linker, respectively. This sensor can be employed to monitor the entire process of the C-reactive protein (CRP) sensing, including antibody modification and antigen detection. The design and the optimization of the optical fiber waveguide-coupled SPR sensor were realized, based on the transfer matrix method and first-principles calculations. The sensor was fabricated and characterized according to the optimized parameters. The experimental setup was implemented to measure the entire process of antibody modification and antigen detection for CRP with the detection limit of 3.21 pmol·mL^{-1}, and the specificity tests were also carried out.

Keywords: Surface plasmon resonance (SPR); dielectric layer; poly-dopamine (PDA); C-reactive protein (CRP)

Citation: Jinying MA, Shixin LI, Xiangdong HUANG, Junfeng JIANG, Tianhua XU, and Tiegen LIU, "All Optic-Fiber Waveguide-Coupled SPR Sensor for CRP Sensing Based on Dielectric Layer and Poly-Dopamine," *Photonic Sensors*, 2025, 15(2), 250224.

1. Introduction

C-reactive protein (CRP) is one of the most important inflammation markers in the human body, which is used in response to infection, tissue inflammation, or other inflammatory stimuli, and can be used to differentiate the infection caused by bacteria from virus clinically [1]. Since the CRP contributes importantly to the diagnosis of human diseases, a number of methods have been developed for its detection, such as enzyme linked immunosorbent assay [2], immunofluorescence assay [3], and latex agglutination [4]. However, these methods have the limitations of being time-consuming, semi-quantitative, and lack of miniaturization.

The optical fiber-based surface plasmon resonance (SPR) sensors have the potential for solving these problems [5]. By the integration of the optical fiber technology and sensor technology, these sensors amalgamate the strengths of both technologies, encompassing enhanced sensitivity, label-free detection, immunity to electromagnetic interference, and electrical insulation. Consequently,

Received: 9 October 2023 / Revised: 16 February 2024

DOI: 10.1007/s13320-024-0734-0
Article type: Regular

such sensors are widely applied in diverse sectors e.g., environmental monitoring, biomedicine, and food security [6]. Since their inception, these sensors have captivated substantial attention and emerged as a focal point for research and development.

The rapid evolution of optical fiber SPR sensors has engendered comprehensive explorations into their architectures [7], materials [8], and sensitivity [9]. Especially, the configuration of the thin film and the selection of materials have been meticulously investigated to enhance the performance and the sensitivity of sensors. As a result, numerous achievements have been attained. These advancements have paved the way for the realization of biological sensing applications. However, there remains a challenge in achieving the dynamic and entire monitoring of the biological sensing process.

To enable practical biological sensing, we successfully developed an all optic-fiber waveguide-coupled SPR sensor, building upon previous research works [10]. This sensor incorporated zirconium disulfide (ZrS_2) as the dielectric layer and poly-dopamine as the biological cross-linker. The design and the optimization of the sensor were achieved through the utilization of transfer matrix methods and first-principles calculations. Subsequently, this SPR sensor was fabricated and characterized based on the optimized parameters. This specifically designed sensor holds the capability to monitor the entire process of the CRP sensing, including antibody modification and antigen detection. Additionally, it allows for the specificity experiments.

2. Principle and optimization

The structure of the all optic-fiber waveguide-coupled SPR sensor is shown in Fig. 1. This sensor design was performed based on a silica-core multimode fiber with the plastic cladding. Key components of the sensor include the optical fiber core, metal layer, and dielectric layer, as shown in Fig. 1(a). The optical fiber core was supposed to be made of silica, while the metal layer could be gold, silver, copper, or aluminum. The dielectric layer was made of new 2-dimensional (2D) materials, such as transition-metal dichalcogenides (TMDCs). In the comparison of different materials for the metal and dielectric layers, gold and zirconium disulfide (ZrS_2) were identified as better choices [10]. The theoretical model of the sensor is described in Fig. 1(b).

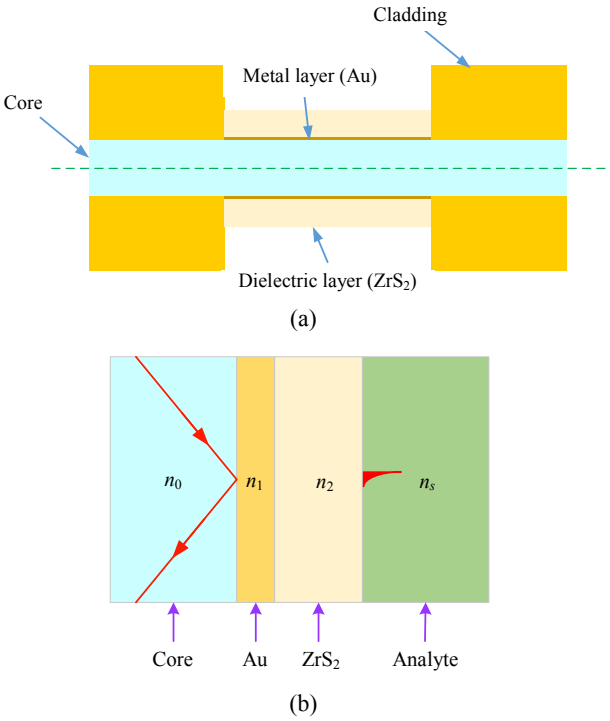

Fig. 1 Structure of the optic-fiber waveguide-coupled SPR sensor: (a) profile view of the whole sensor and (b) theoretical model of the sensor.

The dielectric constants of the optical fiber core and the Au layer could be described according to the Sellmeier dispersion model and the Drude model, respectively [11]. Using the first-principles calculations and the density functional theory, the properties of the ZrS_2 layer could be estimated with the Cambridge Sequential Total Energy Package (CASTEP) module of Materials Studio 7.0, resulting in a dielectric constant that varies with the wavelength [12]. Based on the dielectric constants of each layer, the transmission spectrum characteristics of the all optic-fiber waveguide-coupled SPR sensor were analyzed using

the transfer matrix method [13]. The structure of the sensor shown in Fig. 1(a) could be regarded as a stack of the multi-layer structures with the thickness of d_k and refractive indices of n_k for the kth film layer. The electric and magnetic field amplitudes (E and H) could be expressed using the characteristic matrix equation as [14]

$$\begin{bmatrix} E_1 \\ H_1 \end{bmatrix} = \mathbf{M} \begin{bmatrix} E_N \\ H_N \end{bmatrix} \tag{1}$$

where E_1 and H_1 are the components of the electric and magnetic fields at the boundary of the first layer, E_N and H_N are the components of the electric and magnetic fields of the Nth layer, and **M** denotes the transfer matrix of the multi-layer structure. The transfer matrix **M** can be described as the linear product of the transfer matrix $\mathbf{M}_k$ for the boundary between the kth layer and (k+1)th layer as

$$\mathbf{M} = \prod_{k=0}^{N-1} \mathbf{M}_k = \begin{bmatrix} M_{11} & M_{12} \\ M_{21} & M_{22} \end{bmatrix}. \tag{2}$$

The reflectance R can be calculated as [15]

$$\begin{aligned} R &= |r|^2 \\ &= \left| \frac{(M_{11} + M_{12}\eta_N)\eta_1 - (M_{21} + M_{22}\eta_N)}{(M_{11} + M_{12}\eta_N)\eta_1 + (M_{21} + M_{22}\eta_N)} \right|^2 \end{aligned} \tag{3}$$

where η_k denotes the optical admittance for the kth layer. And the normalized transmitted power, P_{trans}, in the fiber SPR sensor will be then expressed as

$$P_{\text{trans}} = \frac{\int_{\theta_{\text{cr}}}^{\pi/2} R^{N_{\text{ref}}(\theta)} \dfrac{n_0^2 \sin\theta\cos\theta}{\left(1 - n_0^2\cos^2\theta\right)^2} \mathrm{d}\theta}{\int_{\theta_{\text{cr}}}^{\pi/2} \dfrac{n_0^2 \sin\theta\cos\theta}{\left(1 - n_0^2\cos^2\theta\right)^2} \mathrm{d}\theta} \tag{4}$$

where

$$\begin{cases} N_{\text{ref}}(\theta) = \dfrac{L}{D_c \tan\theta} \\ \theta_{\text{cr}} = \sin^{-1}\left(\dfrac{n_{\text{cl}}}{n_0}\right) \end{cases} \tag{5}$$

and θ is the angle of incidence in the fiber core, N_{ref} represents the total number of reflections in the sensing region, while L and D_c represent the length of the exposed sensing region and the diameter of the fiber core, respectively; θ_{cr} is the critical angle of the fiber, whereas n_{cl} is the refractive index of the fiber cladding, and n_0 is the refractive index of the fiber core as shown in Fig. 1(b). And the resonance wavelength (the minimum of the resonance dip of the transmission spectrum of the SPR sensor) λ_{res} can be expressed as [16]

$$\lambda_{\text{res}} = \frac{2\pi c}{\omega_p} \sqrt{\frac{n_0^2(\sin^2\theta) n_s^2 + n_0^2 \sin^2\theta - n_s^2}{n_0^2 \sin^2\theta - n_s^2}} \tag{6}$$

where ω_p=9.03 eV represents the plasma frequency of Au as a constant, n_s is the refractive index of the analyte, and c the speed of light in vacuum. This model enables the theoretical simulation and optimization of the sensor, leading to the optimized parameters for the biological sensing.

It can be seen that (6) is a concave function, so the sensitivity will increase obviously with the refractive index. The refractive indices of most biological solutions are around 1.35 RIU [17]. The length of the sensor was set as 10 mm, while the diameter of the fiber was 600 μm. When the thicknesses of the zirconium disulfide and gold film were set, the transmission spectrum of the sensor could be calculated and the resonance wavelength was extracted, leading to the sensitivity corresponding to different refractive indices of the analyte. When the refractive indices of the analyte were set as 1.35 RIU, the sensitivity of the sensor was simulated as shown in Fig. 2, according to the different thicknesses of the gold and zirconium disulfide film. It can be seen from the figure that the sensitivity is very sensitive to the thickness of the zirconium disulfide film, with the optimized thickness of about 240 nm–260 nm. Meanwhile, the thickness of the gold film could be changed in a relatively wider range. In order to acquire a relatively higher plasmon intensity, the thickness of the gold film was set at 40 nm. When the thickness of the zirconium disulfide film was larger than 320 nm, the sensitivity was reduced because of the energy reduction due to the thicker 2D materials. Deep blue areas indicate zero sensitivity because the

resonance wavelength was beyond the wavelength range of 2000 nm and the fitting curve could not be obtained.

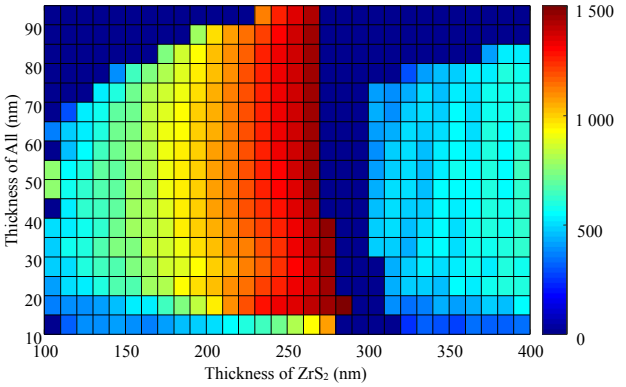

Fig. 2 Sensitivity of the sensor with different gold film depths.

When the thickness of the gold film was set at 40 nm, the thickness of the zirconium disulfide film was varied from 100 nm to 500 nm, leading to the morphologic change of the spectrum. It can be seen from Fig. 3 that, the longer the resonance wavelength is, the deeper the absorbance depth is. When the depth of the zirconium disulfide film was larger than 300 nm, the new resonance mode could be stimulated. When the depth of zirconium disulfide was larger than 400 nm, another new mode could also be stimulated. When the depth was restricted to be less than 300 nm, the resonance valley would be more obvious with the increment of the thickness of the zirconium disulfide film.

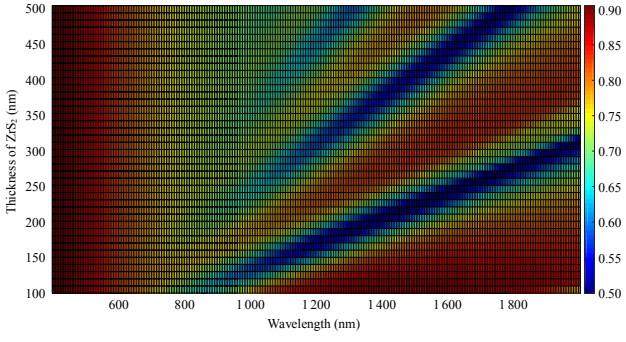

Fig. 3 Transmitted spectrum of the sensor with different zirconium disulfide film depths.

When the thicknesses of the gold and zirconium disulfide film were set at 40 nm and 240 nm, respectively, the transmission spectra of the sensor are shown in Fig. 4(a), and the wavelength shift corresponding to the refractive indices of the analyte is shown in Fig. 4(b). It can be seen from the figure that the fitting curve is a concave function, and the sensitivity increases with the refractive indices.

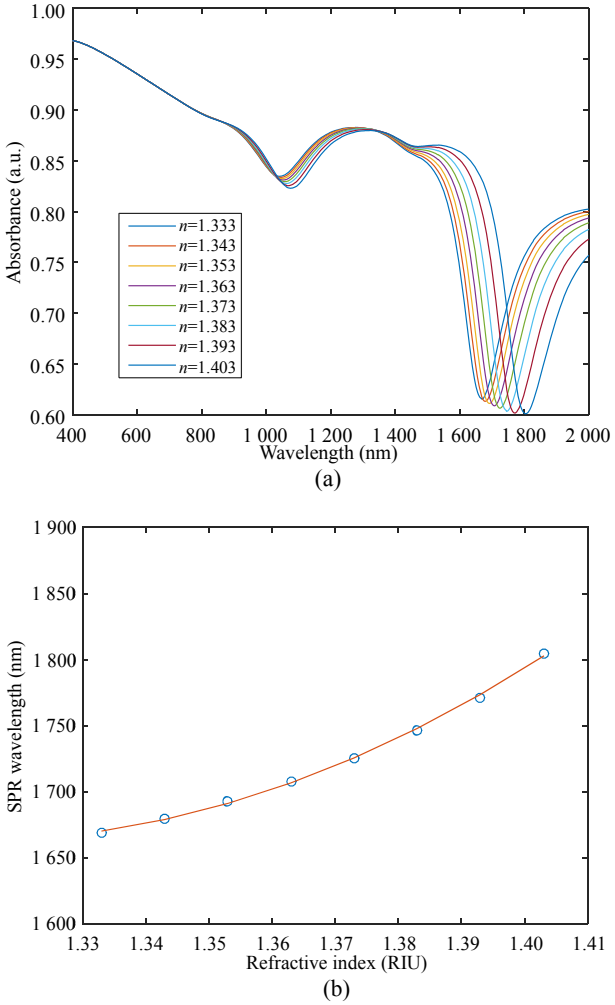

Fig. 4 Transmission spectra and resonance wavelength of the optic-fiber waveguide-coupled SPR sensor: (a) transmission spectra of the sensor and resonance wavelength of the sensor and (b) resonance wavelength of the sensor.

3. Fabrication and characterization

3.1 Sensor fabrication

According to the optimized parameters, the all optic-fiber waveguide-coupled SPR sensor was fabricated for the CRP sensing. This indicated the inflammation degree in the serum monitoring, which is a fundamental biochemical criterion. The fabrication flow chart of the sensor is shown in Fig. 5.

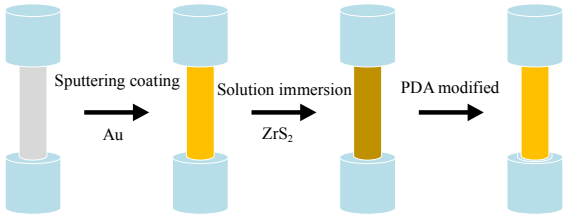

Fig. 5 Fabrication flow diagram of the optic-fiber waveguide-coupled SPR sensor.

The optic-fiber waveguide-coupled SPR sensor was fabricated on a plastic-cladding silica-core multimode fiber, with a numerical aperture of 0.37 and a core diameter of 600 μm, respectively. After being cleaned by acetone and ethanol successively in an ultrasonic cleaner, a ~10 mm unclad section in the middle of the fiber was coated with a 40 nm-thick gold layer, using the vacuum sputtering coating device, in a pure Ar atmosphere under a working pressure of 1 Pa (7.5 mTorr). The completed sensor was immersed into the ultrasound treated ZrS_2 isopropanol nano-dispersion until the full evaporation of the solution, which indicated the completion of one deposition cycle. Deposition cycles were carried out twice by repeating the above evaporation process for the optimized thickness of the ZrS_2 layer. Then, the procedure of annealing at 50 °C for 5 hours was performed to ensure the adhesion strength. As a neurotransmitter, dopamine would lead to the self-polymerization reaction in the environment of the oxygen and weak base, and the poly-dopamine (PDA) would be produced with an adjustable thickness. Therefore, it could be utilized as a biological cross-linking agent. In order to make more biological molecules firmly fixed on the sensor and form a stable and reliable detection film, PDA was used to cross-link the biological molecules to the sensor surface. The practical sensors fabricated with the above process are shown in Fig. 6.

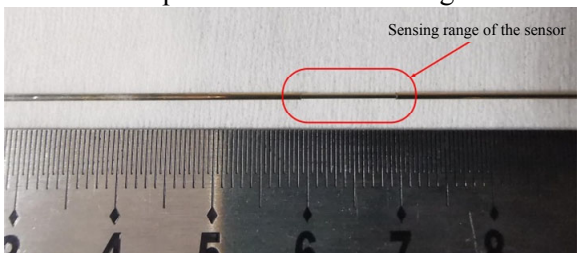

Fig. 6 Practical sensors fabricated with ZrS_2 and PDA layers.

3.2 Characterization of the sensor

To evaluate the performance of the fabricated sensor, it was also characterized by different equipment. The morphology characterization of the Au layer was monitored by the microscope and the atomic force microscope (AFM). The Au layer was very smooth, according to the microscope picture shown in Fig. 7(a). The comparison of the Au layer and bare fiber core was clearly observed in the AFM image shown in Fig. 7(b). The thickness of the Au layer was 43.7 nm with the roughness of 4.46 nm.

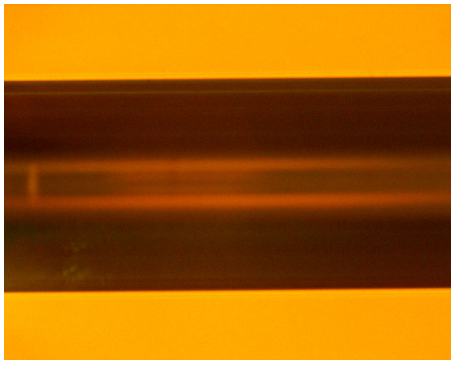

(a)

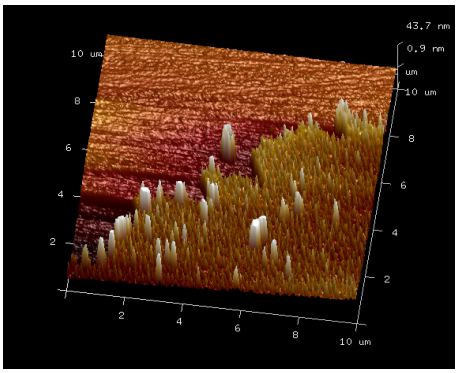

(b)

Fig. 7 Morphology characterization of the Au layer for the optic-fiber waveguide-coupled SPR sensor: (a) microscope picture of the Au layer and (b) AFM picture of the Au layer.

The ZrS_2 layer underwent the characterization using the Raman spectroscopy instrument with a model of HORIBA Scientific LabRAM HR Evolution. Figure 8(a) exhibits the Raman spectrum of the sensor, revealing a wide and asymmetric peak corresponding to the A_{1g} mode at 332 cm^{-1}. This observation was consistent with the data presented in [18], indicating the presence of the ZrS_2 layer. Additionally, the film morphology of the ZrS_2 layer

was examined using the scanning electron microscopy (SEM) at a magnification of 50000×, as depicted in Fig. 8(b). The SEM image demonstrates the uniform distribution of ZrS_2 nano-sheets, ranging in the size from dozens of nanometers to hundreds of nanometers.

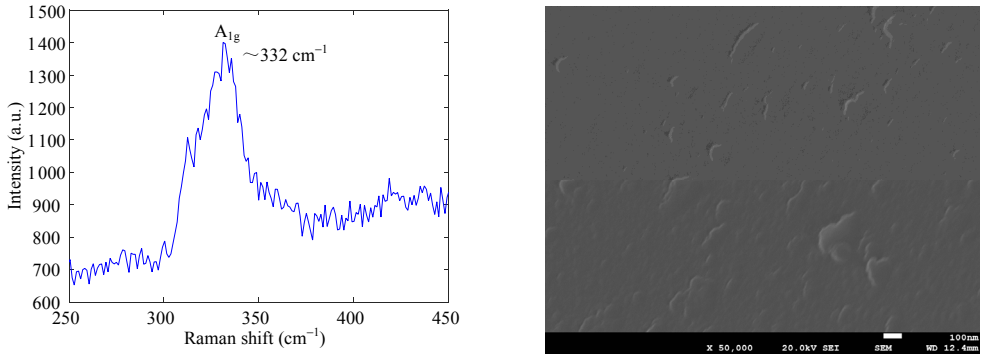

(a) (b)

Fig. 8 Morphology characterization of the ZrS_2 layer for the optic-fiber waveguide-coupled SPR sensor: (a) Raman spectrogram of the ZrS_2 layer and (b) SEM picture of the ZrS_2 layer (50 000×).

To verify the successful modification of the PDA layer onto the sensor surface, a full spectrum scanning of the PDA-functionalized sensor was performed using the X-ray photoelectron spectroscopy (XPS) instrument with a model of Thermo Scientific Escalab 250Xi. The scanning results are shown in Fig. 9(a). The XPS spectrum revealed the presence of carbon (C), nitrogen (N), and oxygen (O) elements on the sensor film layer surface, as well as the presence of amino groups (RNH_2) and imino groups (R_2NH). This characterization experiment confirmed the functionalization of the sensor surface with PDA, which was consistent with previously reported literature [19]. The entire depth of all layers could also be characterized by the SEM, including the Au layer, ZrS_2 layer, and PDA layer. All layers of the sensor were successive and symmetrical, with a total depth of 77 nm as shown in Fig. 9(b). Thus, it could be used in the biological sensing. Additionally, the difference between batches did exist, but the optimized stable process flow could ensure the error within a controllable range, which would have little influence on the performance of the sensors.

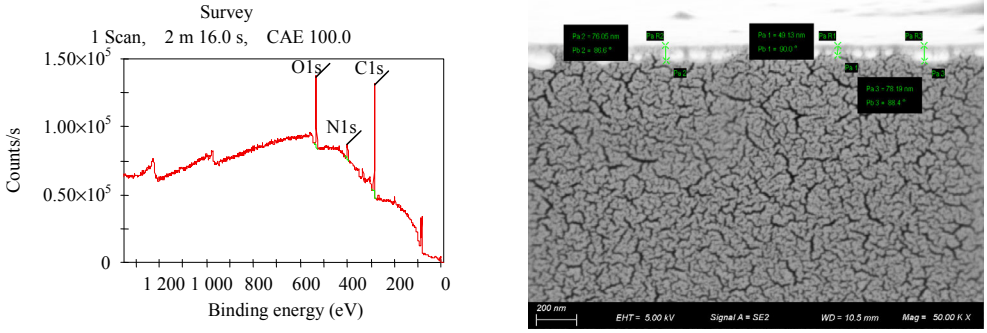

(a) (b)

Fig. 9 Morphology characterization of the PDA layer for the optic-fiber waveguide-coupled SPR sensor: (a) XPS spectrogram of the PDA layer and (b) SEM cross-section picture of the whole layer (50000×).

4. Fabrication and characterization

4.1 Experimental setup

The optic-fiber waveguide-coupled SPR sensing system was implemented, as shown in Fig. 10. It consisted of four parts. The source launched the light into the optic-fiber waveguide-coupled SPR sensor. The detected transmission spectrum of the sensor could be analyzed using the computer. The sensor was immersed into the CRP solution for

monitoring. The transmission spectrum was denoised using all-phase filters [20], resulting in the resonance wavelength of the sensor as the valley position of the spectrum.

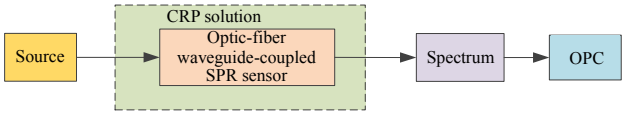

(a)

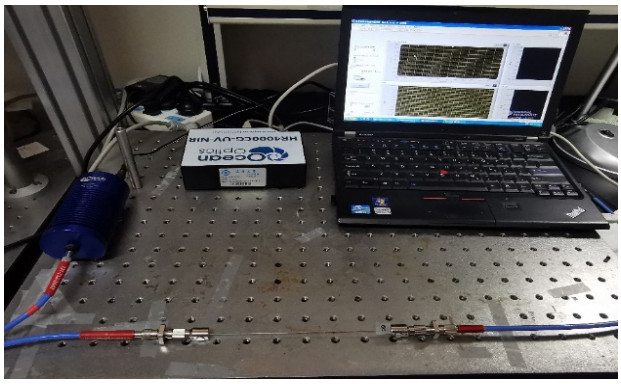

(b)

Fig. 10 Setup and practical system for optic-fiber waveguide-coupled SPR sensing: (a) sensing system setup of the optic-fiber waveguide-coupled SPR sensor and (b) practical experimental field of the optic-fiber waveguide-coupled SPR sensor.

4.2 Experiments and discussion

4.2.1 Sensitivity experiments

To cross-link the biological molecules to the sensor surface, the PDA was used as the biological cross-linking agent. However, it was hard to simulate the performance of the PDA layer. So, the sensitivity investigation of different PDA layer positions could be used to evaluate the effect of the PDA. Five sensors were fabricated with structures of the Au layer only, Au layer+ZrS_2 layer, Au layer+PDA layer, Au layer+PDA layer+ZrS_2 layer, and Au layer+PDA layer+ZrS_2 layer+PDA layer, respectively. These five sensors could be used for the refractive index monitoring with the system setup as shown in Fig. 10.

When the refractive index was changed from 1.34 RIU to 1.38 RIU, the resonance wavelengths of different sensors are shown in Fig. 11(a). The relationship between the resonance wavelength and the refractive index was fitted based on the inverse proportional function. Using the fitting results, the sensitivity of the sensors corresponding to different refractive index values could be calculated as Fig. 11(b). The PDA layer and the ZrS_2 layer would both cause the redshift of the resonance wavelength for the SPR sensor, and both factors could be superposed. When both layers were used, the sensitivity would increase sharply. When the refractive index was larger than 1.375 RIU, the sensor with the Au layer+PDA layer+ZrS_2 layer had the highest sensitivity, and the highest value could reach 9 500 nm/RIU when the refractive index was 1.39 RIU. As the spectrometer had the resolution of 0.02 nm, the refractive index resolution of the sensor could reach 2.1×10^{-6} RIU with the best performance. When the refractive index was smaller than 1.375 RIU, the sensor with the Au layer+PDA layer+ZrS_2 layer+PDA layer had the highest sensitivity. As the biological solution usually had the refractive index of around 1.35 RIU [17], we used the sensor with the structure of the Au layer+PDA layer+ZrS_2 layer+PDA layer for the biological sensing application. Additionally, further stacking of the PDA layer+ZrS_2 layer would increase the sensitivity of the sensor and also broaden the transmission spectrum of the sensor at the same time, leading to large errors in the SPR wavelength demodulation or even fail to detect the SPR valley.

Table 1 shows the performance comparison between the sensors proposed in this work and some other technologies. It could be seen that the sensors with the structure proposed in this work had the highest sensitivity with the widest detection range. This was because the PDA layer outside of the ZrS_2 layer had the stronger adsorption ability for the analyte, especially biological molecules.

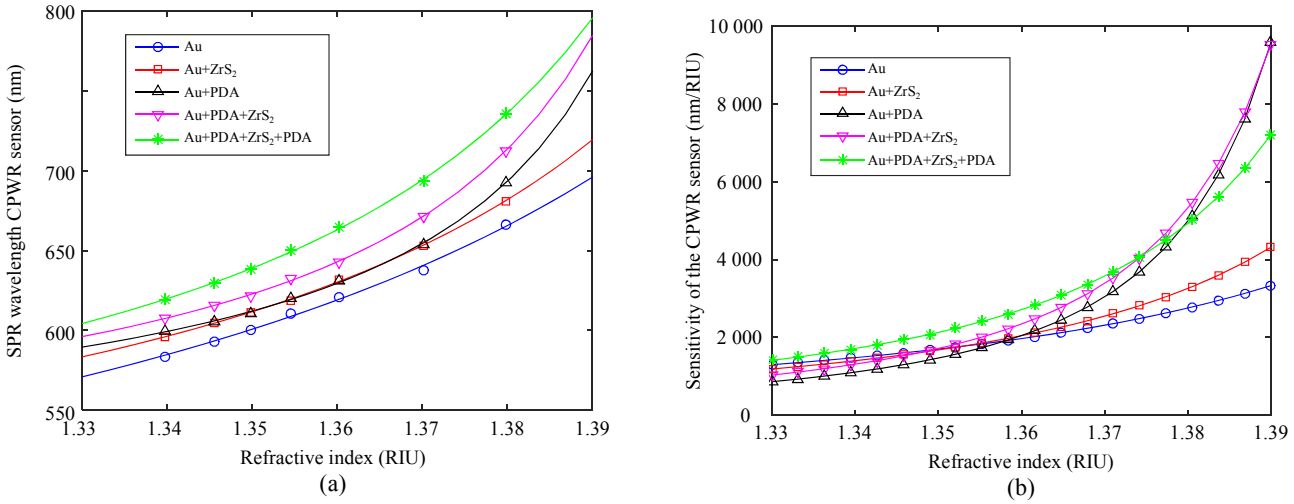

Fig. 11 Resonance wavelength and the sensitivity of the optic-fiber waveguide-coupled SPR sensor: (a) resonance wavelength of the sensor and (b) sensitivity of the sensor.

Table 1 Performance comparison of different fibers based SPR sensors.

Sensing structure	Refractive index range (RIU)	Sensitivity (nm/RIU)	Ref.
Fiber core/Ag layer/Pt layer/ITO/graphene/analyte	1.33–1.36	4 150	[21]
Fiber core/Ag layer/Au layer/MoS_2/analyte	1.331 8–1.370 1	3 061.84	[22]
Fiber/MoS_2/Au layer/analyte	1.331 4–1.362 3	6 184.40	[23]
Fiber core/Cr layer/Au layer/$MoSe_2$/analyte	1.333–1.358	2 793.36	[24]
Fiber core/Al layer/graphene/MoS_2/analyte	1.330–1.332	6 200	[25]
Fiber core/Au layer/PDA layer/ZrS_2/analyte	1.33–1.39	9 500	This work

4.2.2 Entire processing monitoring of the CRP immunoreaction

The immunoreaction between the anti-CRP molecule and the CRP molecule would cause the change of the refractive index. The optic-fiber waveguide-coupled SPR sensor with the Au layer+PDA layer+ZrS_2 layer+PDA layer was used in the CRP immunoreaction sensing. The anti-CRP was immobilized onto the surface of the sensor to realize the functionalization, with bovine serum albumin (BSA) blocking to enhance the performance of the sensor. The entire process including the functionalization and sensing are shown as Fig. 12, and also could be monitored by the optic-fiber waveguide-coupled SPR sensor.

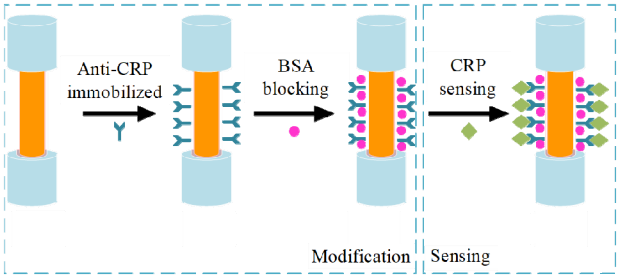

Fig. 12 Functionalization of the optic-fiber waveguide-coupled SPR sensor for CRP immunoreaction sensing.

We executed the detection of the CRP serum solution with different concentrations. The refractive index of the CRP serum solution was measured by the Abbe refractometer, and the result was about 1.3456 RIU. When the concentration of the CRP serum solution changed from 10 μmol·mL^{-1} to 500 μmol·mL^{-1}, the average values of 100 times of measurement were calculated, with the mean square error no more than 0.17 nm. The relationship

between the SPR wavelength and the concentration of the CRP serum solution is shown as Fig. 13. It can be seen that the relationship between them is nearly linear, and the slope of the curve is 52.9 nm/(nmol·mL^{-1}), leading to the concentration resolution reaching 3.21 pmol·mL^{-1} for the serum solution of the CRP, with the maximum wavelength error below 0.17 nm. We also compared the performance of the sensor with other CRP sensors, and the results are shown in Table 2, in terms of the detection range and detection limit. It could be seen that the sensor proposed in this work had the best detection limit for the CRP detection, and the value was only one third of the latest reference [29].

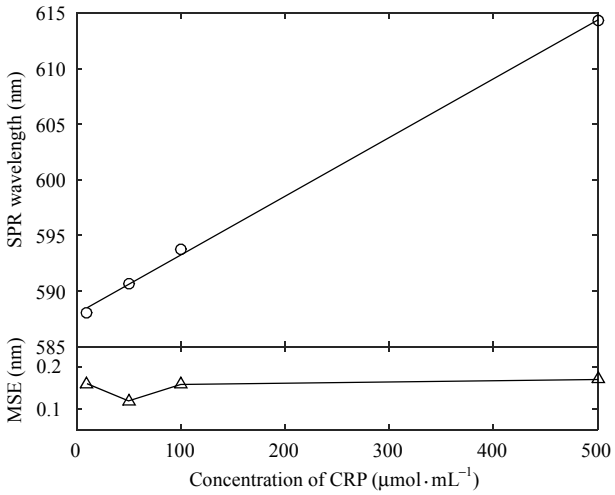

Fig. 13 SPR wavelength response of the sensor for the serum solution of the CRP with different concentrations.

Table 2 Performance comparison of CRP detection based on different methods.

Sensing structure	Detection range (μmol·mL^{-1})	Detection limit (pmol·mL^{-1})	Ref.
Fiber core/magnetic nanoparticles	450–6 500	400	[26]
Fiber core/gold nanoparticles	40–900	52.2	[27]
Fiber/bioresponsive hydrogel	0–2 100	46.5	[28]
Fiber core/Cr layer/ Au layer/PDA-NPs/analyte	0–340	9.57	[29]
Fiber core/Au layer/PDA layer/ ZrS_2/analyte	10–500	3.21	This work

The entire process of sensor functionalization and immunoreaction sensing is shown in Fig. 14. The sensor was immersed in pure water for Processes 1 and 3. The wavelengths were basically the same for both processes, which indicated that the performance of the sensor was stable. The anti-CRP immobilization on the sensor surface was carried out in Process 4. It could be seen that the wavelength of the sensor shifted very slowly, which meant that the functionalization of the sensor required more time. The BSA blocking occurred in Process 5, in order to eliminate the superfluous active spots. As the antibodies and antigens should be both dissolved in the phosphate buffer saline (PBS) solution, the sensor should be cleaned by the PBS solution as a reference liquid before the anti-CRP immobilization and after the BSA blocking, respectively. These two operations could be clearly observed in Processes 2 and 6. The wavelength difference between these two processes meant that the anti-CRP molecules were immobilized on the surface of the sensor successfully. The immunoreaction between the anti-CRP and the CRP molecules was shown in Process 7. The figure showed that the wavelength shift was fast at the earlier process while lower at the later time. After the immunoreaction, the sensor was also immersed into the PBS solution, as illustrated in Process 8. As the obvious wavelength difference between Processes 6 and 8 for the same PBS solution, it could be concluded that the immunoreaction occurred adequately. After being cleaned by the PBS solution in Process 8, the sensor was also immersed into the pure water during Process 9. The large difference between the wavelengths in Processes 9 and 1 also verified the immunoreaction. Process 10 referred to the final immersing operation of the sensor in the PBS solution. The SPR wavelengths in

Processes 8 and 10 were nearly the same, which meant that the binding of anti-CRP and CRP molecules was strong and was not dropped when cleaned by the pure water. All in all, the optic-fiber waveguide-coupled SPR sensor could effectively monitor the entire process of the sensor functionalization and the immunoreaction sensing.

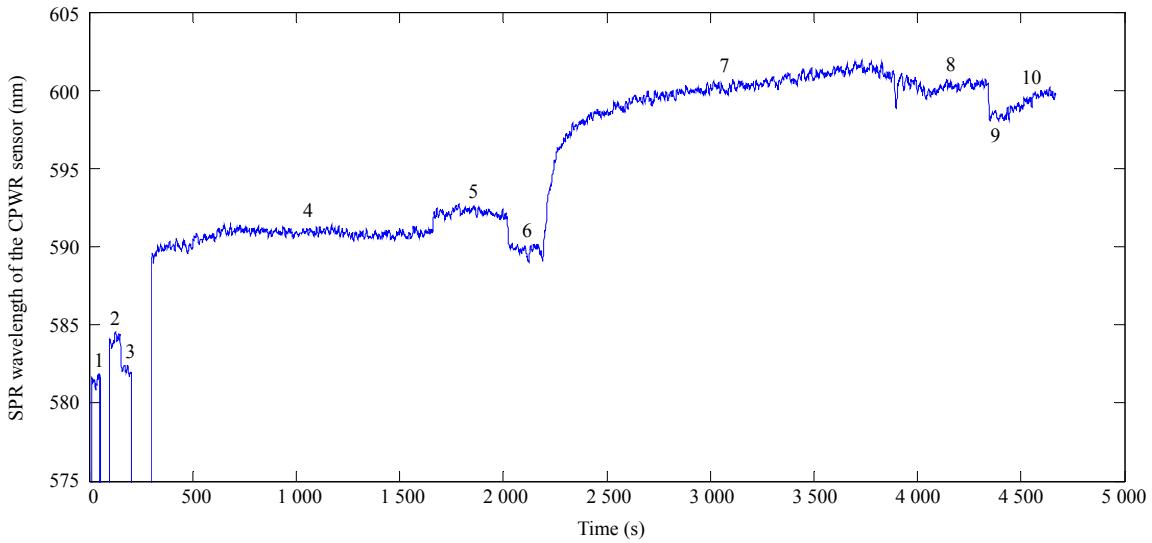

Fig. 14 Entire process of sensor functionalization and immunoreaction sensing (the numbers 1–10 indicate Process 1 to Process 10).

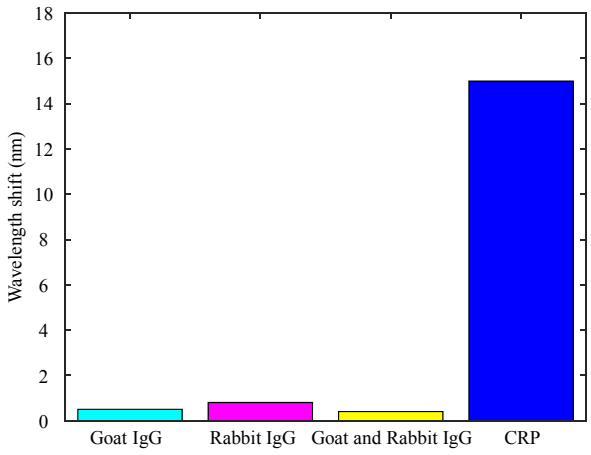

Fig. 15 Wavelength shifts in different solutions for the sensor immobilized by anti-CRP.

4.2.3 Specificity experiments

To verify the specificity of the senor, the anti-CRP immobilized sensors were immersed into different solutions and the wavelength shifts were detected separately. These solutions included goat IgG, rabbit IgG, goat anti rabbit IgG, and CRP solutions, respectively. These solutions had the same concentration of 0.05 mg/mL. The experimental processes were the same, and the maximum wavelength shifts were recoded as shown in Fig. 15. Only the CRP solution caused a wavelength shift of 15 nm, while all other solutions produced the wavelength shifts of no more than 1 nm. It indicated that the sensor had a good specificity detection ability, which could be applied in the immunological detection effectively in the mixed solution.

5. Conclusions

We developed an all optic-fiber waveguide-coupled SPR sensor using the ZrS_2 and PDA as the dielectric layer and the biological cross-linker, respectively. The design and the optimization of the optical fiber waveguide-coupled SPR sensor was realized, based on the transfer matrix method and the first-principles calculations, leading to the optimized parameters of Au and ZrS_2 film depths of 40 nm and 240 nm, respectively. The sensor was fabricated and characterized according to these optimized parameters. This sensor could be used to monitor the entire process of the CRP sensing,

including the antibody modification and the antigen detection. The experimental setup was implemented, and the entire process of the antibody modification and the antigen detection for the CRP was monitored and analyzed, leading to detection limit of 3.21 pmol·mL^{-1}. The specificity experiments have also been performed.

Acknowledgment

This work was funded by the National Key Research and Development Program of China (Grant No. 2022YFF0706003) and National Natural Science Foundation of China (Grant No. 62375202).

We thank Prof. Liang XU and Rui SU from Tianjin Second People's Hospital to provide the serum sample of CRP for experiments. We also thank the Bioss Antibodies Company for the product of CRP.

Declarations

Ethics Approval and Consent to Participate Experimental processes were supervised by Tianijn University, China. The collection and utilization of the datasets were approved by the Ethics Committee on Biomedical Research, Tianjin Second People's Hospital (No.2024-037). All approaches performed in the study involving data collection and storage were followed according to the standard operation process of Recombinant Human CRP protein Specifications issued by the Bioss Antibodies Company. And the product batch number is bs-0391P.

Conflict of Interest The authors declare that they have no competing interests.

Permissions All the included figures, tables, or text passages that have already been published elsewhere have obtained the permission from the copyright owner(s) for both the print and online format.

References

[1] W. Wang, Z. Mai, Y. Chen, J. Wang, and L. Li, "A label-free fiber optic SPR biosensor for specific detection of C-reactive protein," *Scientific Reports*, 2017, 7: 16904.

[2] N. Barka, J. Tomasi, and S. Stadtsbaeder, "Use of whole Streptococcus pneumoniae cells as a solid phase sorbent for C-reactive protein measurement by ELISA," *Journal of Immunological Methods*, 1985, 82(1): 57–63.

[3] H. Harma, J. Toivonen, and J. Soini, "Time-resolved fluorescence immunoassay for C-reactive protein using colloidal semiconducting nanoparticles," *Sensors*, 2011, 11(12): 11335–11342.

[4] O. Senju, Y. Takagi, and R. Uzawa, "A new immuno quantitative method by latex agglutination – application for the determination of serum C-reactive protein (CRP) and its clinical significance," *Journal of Clinical Immunology*, 1986, 19(2): 99–103.

[5] A. Sharma, R. Jha, and B. Gupta, "Fiber-optic sensors based on surface plasmon resonance: a comprehensive review," *IEEE Sensors Journal*, 2007, 7(8): 1118–1129.

[6] J. Ma, T. Liu, J. Jiang, K. Liu, S. Wang, and Z. Zhang, "Progress in sensitivity enhancement for optical fibre surface plasmon resonance sensing," *Chinese Journal of Lasers*, 2021, 48(19): 1906002.

[7] Y. Zhang, C. Liao, C. Lin, Y. Shao, and Y. Wang, "Surface plasmon resonance refractive index sensor based on fiber-interface waveguide inscribed by femtosecond laser," *Optics Letters*, 2019, 44(10): 2434–2437.

[8] S. Lee, H. Song, and H. Ahn, "Fiber-optic localized surfacer plasmon resonance sensors based on nanomaterials," *Sensors*, 2021, 21(3): 819.

[9] J. Jing, K. Liu, J. Jiang, T. Xu, S. Wang, and J. Ma, "Performance improvement approaches for optical fiber SPR sensors and their sensing applications," *Photonics Research*, 2022, 10(1): 126–147.

[10] J. Jing, K. Liu, J. Jiang, T. Xu, S. Wang, and P. Chang, "All optic-fiber coupled plasmon waveguide resonance sensor using ZrS_2 based dielectric layer," *Optics Express*, 2020, 28(8): 11280–11289.

[11] S. Shukla, N. K. Sharma, and V. Sajal, "Theoretical study of surface plasmon resonance-based fiber optic sensor utilizing cobalt and nickel films," *Brazilian Journal of Physics*, 2016, 46(3): 288–293.

[12] R. Evarestov and A. V. Bandura, "First-principles calculations of single-walled nanotubes in sulfides MS_2 (M=Ti, Zr)," *Physica Scripta*, 2014, 89(4): 044001.

[13] J. Ma, K. Liu, J. Jiang, T. Xu, S. Wang, and P. Chang, "Theoretical and experimental investigation of an all-fiber waveguide coupled surface plasmon

resonance sensor with Au-ZnO-Au sandwich structure," *IEEE Access*, 2019, 7: 169961.

[14] K. Tiwari, S. C. Sharma, and N. Hozhabri, "High performance surface plasmon sensors: simulations and measurements", *Journal of Applied Physics*, 2015, 118(9): 093105.

[15] A. Sharma, R. Jha, and B. Gupta, "Influence of dopants on the performance of a fiber optic surface plasmon resonance sensor", *Optics Communications*, 2007, 274(2): 320–326.

[16] J. Jing, K. Liu, J. Jiang, T. Xu, and S. Wang, "Highly sensitive and stable probe refractometer based on configurable plasmonic resonance with nano-modified fiber core", *Opto-Electron Advanced*, 2023, 6(6): 220072.

[17] S. Cao, Y. Shao, Y. Wang, T. Wu, and L. Zhang, "Highly sensitive surface plasmon resonance biosensor based on a low-index polymer optical fiber", *Optics Express*, 2018, 26(4): 3988–3994.

[18] M. Mattinen, G. Popov, and M. Vehkamaki, "Atomic layer deposition of emerging 2D semiconductors, HfS_2 and ZrS_2, for optoelectronics," *Chemistry of Materials*, 2019, 31(15): 5713–5724.

[19] A. Alkhouzaam and H. Qiblawey, "Novel polysulfone ultrafiltration membranes incorporating polydopamine functionalized graphene oxide with enhanced flux and fouling resistance," *Journal of Membrane Science*, 2021, 620: 118900.

[20] Y. Cao, J. Ma, K. Liu, X. Huang, and J. Jiang, "Optical fiber SPR sensing demodulation algorithm based on all-phase filters," *Acta Physica Sinica*, 2017, 66(7): 120–126.

[21] M. Alagdar, B. Yousif, N. F. Areed, and M. Elzalabani, "Highly sensitive fiber optic surface plasmon resonance sensor employing 2D nanomaterials," *Applied Physics A – Materials Science & Processing*, 2020, 126: 522.

[22] Q. Wang, X. Jiang, L. Niu, and X. Fan, "Enhanced sensitivity of bimetallic optical fiber SPR sensor based on MoS_2 nanosheets," *Optics and Lasers in Engineering*, 2020, 128: 105997.

[23] H. Song, Q. Wang, and W. M. Zhao, "A novel SPR sensor sensitivity-enhancing method for immunoassay by inserting MoS_2 nanosheets between metal film and fiber," *Optics and Lasers in Engineering*, 2020, 132: 106135.

[24] K. Liu, J. Zhang, J. Jiang, T. Xu, S. Wang, and P. Chang, "$MoSe_2$-Au based sensitivity enhanced optical fiber surface plasmon resonance biosensor for detection of goat-anti-rabbit IgG," *IEEE Access*, 2020, 8: 660–668.

[25] A. Mishra, S. Mishra, and R. Verma, "Graphene and beyond graphene MoS_2: a new window in surface-plasmon-resonance-based fiber optic sensing," *Journal of Physical Chemistry C*, 2016, 120: 2893–2900.

[26] Y. Lin, J. Yang, T. Shu, T. Lin, Y. Chen, M. Su, W. Li, and M. Liu, "Detection of C-reactive protein based on magnetic nanoparticles and capillary zone electrophoresis with laser-induced fluorescence detection," *Journal of Chromatography A*, 2013, 1315: 188–194.

[27] M. Antonio, R. Ferreira, and R. Vitorino, "A simple aptamer-based colorimetric assay for rapid detection of C-reactive protein using gold nanoparticles," *Talanta*, 2020, 214: 120868.

[28] M. Lucio, A. Montoto, and E. Fernandez, "Label-free detection of C-reactive protein using bioresponsive hydrogel-based surface relief diffraction gratings," *Biosens Bioelectron*, 2021, 193: 113561.

[29] G. Cao, P. Chang, A. Zhang, F. Liu, and H. Pan, "A polydopamine nanospheres modified fiber optic SPR biosensor for specific detection of C-reactive protein," *Optical Fiber Technology*, 2023, 80: 103468.